



1 **Method to Quantify the Black Carbon Aerosol Light Absorption Enhancement with Entropy**
2 **and Diversity Measures**

3 Gang Zhao¹, Tianyi Tan¹, Yishu Zhu¹, Min Hu¹, Chunsheng Zhao^{2*}

4 ¹ State Key Joint Laboratory of Environmental Simulation and Pollution Control, International Joint
5 Laboratory for Regional Pollution Control, Ministry of Education, College of Environmental
6 Sciences and Engineering, Peking University, Beijing, 100871, China

7 ² Department of Atmospheric and Oceanic Sciences, School of Physics, Peking University, Beijing,
8 100871, China

9 *Correspondence author: Chunsheng Zhao (zcs@pku.edu.cn)

10 **Abstract**

11 Large uncertainties remain when estimating the warming effects of ambient black carbon (BC)
12 aerosols on climate. One of the key challenges in modeling the radiative effects is predicting the BC
13 light absorption enhancement, which is mainly determined by its mass ratio of non-BC coating
14 thickness to BC (MR). For the same MR, recent researches find that the radiative absorption
15 enhancements by BC are also controlled by its particle-to-particle heterogeneity. In this study, the
16 BC mixing state index (χ) is developed to quantify the dispersion of ambient black carbon aerosol
17 mixing states based on binary systems of BC and other non-black carbon components. We
18 demonstrate that the BC light absorption enhancement increases with χ for the same MR, which
19 indicates that χ can be employed as a factor to constrain the light absorption enhancement of ambient
20 BC. Our framework can be further used in the model to study the black carbon radiative effects on
21 climate change.

22

23 **1 Introduction**

24 Black carbon (BC) aerosols absorb solar radiation, thus exert warming effects on the earth's
25 energy system (Bond and Bergstrom, 2006; Bond et al., 2013). However, large uncertainties remain
26 when quantifying the BC warming effects (Cui et al., 2016; Jacobson, 2010; Koch et al., 2009; Menon



27 et al., 2002). Most of the BC particles were emitted from incomplete combustion of bio fossil fuel
28 (Bond et al., 2013). After initially emitted, the BC particles would experience aging processing with
29 some other non-BC components coated on the BC particles (Peng et al., 2017; Peng et al., 2016).
30 During the aging processing, the light absorption of BC aerosols would increase, which is well
31 known as “lensing effects” (Saleh et al., 2013; Saleh et al., 2014). One critical challenge in estimating
32 the BC warming effects is quantifying the “lensing effects” of ambient BC aerosols (Liu et al., 2017).

33 The light absorption enhancement (E_{abs}), which is the ratio of light absorption of BC aerosols
34 with the coating to that of bare BC particles, is proposed to quantify the “lensing effects”.
35 Comprehensive studies have been carried out to study the E_{abs} (Liu et al., 2017; Peng et al.,
36 2016; Liu et al., 2015; Fierce et al., 2016; Fierce et al., 2020; Cappa et al., 2012). However, a large
37 discrepancy remains between the results of E_{abs} from field measurements and laboratory studies.
38 The measured E_{abs} of laboratory generated monodisperse BC particles can reach up to a factor of 2,
39 which is consistent with the results from the Mie scattering model (Cappa et al., 2012; Cappa et al.,
40 2019). However, some field measurement shows that the E_{abs} of ambient BC aerosols are relatively
41 small, with 1.06 at California (Cappa et al., 2012), 1.07 in South China (Lan et al., 2013), and 1.10 in
42 Japan (Nakayama et al., 2014), while the measured E_{abs} of ambient BC reaches 1.59 during
43 summer time in Beijing (Xie et al., 2019).

44 Many factors, such as the morphology of the BC core, the position of BC core inside coating, the
45 coating thickness, and size distribution of the BC, would influence the E_{abs} of ambient BC aerosols.
46 Wu et al. (2018) reported that the BC light absorption properties vary significantly for different
47 morphology from the calculation of models. Laboratory studies also find that the light absorption
48 properties of the BC core were tuned due to the change of the BC core morphology (Yuan et al.,
49 2020). Comparing with the concentric spherical structure, the off-center coated BC aggregates would
50 lead to up to a 31% reduction in E_{abs} by the multiple-sphere T-matrix method (Zhang et al., 2017).
51 It has been well studied that the E_{abs} is highly related with the mass ratio of coating materials and
52 BC core (MR) (Liu et al., 2014; Liu et al., 2017). Zhao et al. (2019b) reported that the light



53 absorption properties of ambient BC particles are influenced by BC mass size distribution. Besides,
54 recently researchers found that the E_{abs} are also controlled by particle-to-particle heterogeneity
55 (Fierce et al., 2016; Fierce et al., 2020). As shown in Fig.1, the E_{abs} of ambient aerosols for the
56 same MR would vary by about 30%, which is consistency with the results of Fierce et al. (2020).
57 However, there is no study, to our best knowledge, that constrains the uncertainties of the E_{abs} for
58 the same MR.

59 In this study, we developed a BC mixing states index (χ) to quantify the dispersion of black
60 carbon aerosol mixing states based on binary systems of BC and other non-black carbon components.
61 We demonstrate that the BC E_{abs} increases with χ for the same MR based on the field measurement,
62 which indicates that χ can be employed as a factor to constrain the E_{abs} properties of ambient BC.

63 2 Data and methods

64 2.1 Field measurement

65 The field measurements were conducted at a suburban site Taizhou (119°57' E, 32°35' N) from
66 26 May to 18 June. As shown in Fig. S1, the Taizhou site lies between two large cities of Nanjing
67 and Shanghai, where the aerosols can be seen as representative that of the Yangtze River Delta area
68 (Liu et al., 2020). More details of the field measurements can refer to Zhao et al. (2019a). During the
69 field measurement, we placed all of the instruments in a container where the temperature was
70 carefully controlled between 22 and 26 °C. A PM₁₀ impactor, which is about 5 meters above the
71 ground, was mounted on the top of the container. The sample aerosols were drawn from the impactor
72 and then dried by a Nafion dryer tube.

73 The size-resolved BC mixing states were measured by using a differential mobility analyzer
74 (DMA, model 3081, TSI, USA) in tandem with a single-particle soot photometer (SP2, Droplet
75 Measurement Technologies, USA). Detailed information on the DMA can refer to Zhao et al.
76 (2019c). SP2 can measure the BC mass concentration from the incandescence signals emitted by the
77 BC particle, which is heated to around 6000 K by laser with a wavelength of 1064 nm (Zhao et al.,
78 2020b). Along with the measurement of size-resolved BC mixing states, a nephelometer (Aurora 300,



79 Ecotech, Australia) (Müller et al., 2011) was employed to measure the aerosol scattering coefficient
80 (σ_{sca}) at the wavelength of 525 nm.

81 **2.2 BC mixing states from DMA-SP2 system**

82 In this study, the SP2 was placed after the DMA to measure the size-selected mixing states of the
83 quasi-monodisperse aerosols. The schematic instrument setup is shown in Fig. S1 and the details can
84 refer to part 1 in the supplementary material. After careful calibrations of the SP2 (part 2.1 in the
85 supplementary material), transformations of the measured signals to BC mass concentrations (part
86 2.2 in the supplementary material), and multiple charging corrections (part 2.3 in the supplementary
87 material), the BC-containing number concentration distribution under different total diameter (D_p)
88 and BC core diameter (D_c) can be calculated, as shown in Fig. S4 (b). The details of the calculation
89 of size-resolved BC mixing states from the DMA-SP2 system can refer to Zhao et al. (2020a). The
90 measured size-resolved BC mixing states as in Fig. S4(b) were used for further analysis. It should be
91 mentioned that the measured number distribution of BC-containing aerosols is two dimensional

92
$$\left(\frac{dN}{d\log D_p \cdot d\log D_c}\right).$$

93 **2.3 Calculating the aerosol optical properties**

94 **2.3.1 Calculating the aerosol absorption coefficient for a given D_p and D_c**

95 A Mie scattering model (Bohren and Huffman, 2007) was employed to calculate the aerosol
96 absorption coefficient (σ_{abs}). When calculating the σ_{abs} of single particle, the Mie scattering model
97 requires the diameter of the core, the coating thickness, the refractive index of the core, and the
98 refractive index of the shell. The refractive index of the core adopted here is $1.67+0.67i$, which is the
99 calculated mean value by comparing the measured light absorption and calculated light absorption
100 properties (Zhao et al., 2020a). The refractive index of the shell is chosen to be $1.46+0i$, which is
101 assumed to be as that of the non-BC component measured by the DMA-SP2 system (Zhao et al.,
102 2019a; Zhao et al., 2019c). With the above information, the σ_{abs} values at a given D_p and a given D_c
103 can be calculated.



104 2.3.2 Calculating the aerosol bulk absorption coefficient

105 We calculate the single-particle σ_{abs} of different D_p and D_c with the given refractive index of
106 core and shell and then the ambient aerosol σ_{abs} distributions at different D_p and D_c ($\frac{d\sigma_{abs}}{d\log D_p \cdot d\log D_c}$)
107 can be calculated by multiplying the number concentrations of the BC-contained aerosols
108 ($\frac{dN}{d\log D_p \cdot d\log D_c}$). By integrating the $\frac{d\sigma_{abs}}{d\log D_p \cdot d\log D_c}$ over different D_c values, the ambient aerosol σ_{abs}
109 distribution along with different D_p ($\frac{d\sigma_{abs}}{d\log D_p}$) can be calculated. The total σ_{abs} of the ambient
110 BC-containing aerosols can be calculated by integrating the $\frac{d\sigma_{abs}}{d\log D_p}$ over different D_p values.

111 2.3.3 Calculating the aerosol E_{abs}

112 Along with calculating the σ_{abs, D_p, D_c} of single-particle for different D_p and D_c , we calculate the
113 corresponding light absorption (σ_{abs, D_c, D_c}) value for D_c without thickness. The corresponding total
114 light absorption of all measured BC-contained aerosols without thickness can be calculated by
115 integrating the calculated σ_{abs, D_c, D_c} among different D_p and D_c weighted with $\frac{dN}{d\log D_p \cdot d\log D_c}$. Thus
116 the ambient BC particles without coating ($\sigma_{abs, D_p=0}$) can be calculated. The bulk ambient aerosol
117 E_{abs} can thus be calculated with $E_{abs} = \frac{\sigma_{abs}}{\sigma_{abs, D_p=0}}$.

118 2.4 Quantifying the dispersion of BC mixing states

119 As for BC particles with known D_p and D_c , the mass concentration of BC core and coating
120 material can be calculated with the effective density of BC core and coating material. The effective
121 density of the BC core is calculated in detail in section 2.2 in the supplement. The effective density
122 of the coating material is assumed to be the same as the measured effective density of non-BC
123 aerosols by using a centrifugal particle mass analyzer (version 1.53, Cambustion Ltd, UK) in tandem
124 with a scanning mobility particle sizer system (Zhao et al., 2019a) and a mean value of 1.5 g/cm³ was
125 used here.



126 For each of the particle i ($i=1,2,\dots, N$ is the measured BC-containing aerosol number
127 concentration), we can calculate its mass ratio of BC with

$$128 \quad p_{i,BC} = \frac{m_{i,BC}}{m_i}, \quad (1)$$

129 where $m_{i,BC}$ is the mass concentration of BC and m_i is the total mass concentration of particle i .

130 The mass portion of BC can be calculated as

$$131 \quad p_{BC} = \frac{m_{BC}}{m_{tot}}, \quad (2)$$

132 where m_{BC} (the total mass concentration of BC) and m_{tot} (total mass of BC-containing aerosols)

133 can be calculated as $m_{BC} = \sum_{i=1}^N m_{i,BC}$, $m_{tot} = \sum_{i=1}^N m_i$. The MR is calculated as:

$$134 \quad MR = \frac{(m_{tot}-m_{BC})}{m_{BC}}, \quad (3)$$

135 The mass portion of particle i to total BC-containing aerosols is calculated as

$$136 \quad p_i = \frac{m_i}{m_{tot}}. \quad (4)$$

137 With the definition above, we can calculate the mixing entropy of particle i (H_i) by:

$$138 \quad H_i = -(p_{i,BC} \ln(p_{i,BC}) + (1 - p_{i,BC}) \ln(1 - p_{i,BC})), \quad (5)$$

139 the average mixing entropy of each particle by:

$$140 \quad H_\alpha = \sum_{i=1}^N p_i H_i, \quad (6)$$

141 And the population bulk mixing entropy by:

$$142 \quad H_\gamma = -(p_{BC} \ln(p_{BC}) + (1 - p_{BC}) \ln(1 - p_{BC})). \quad (7)$$

143 Then the average particle species diversity can be calculated by

$$144 \quad D_\alpha = e^{H_\alpha}, \quad (8)$$

145 And the bulk population species diversity can be calculated by

$$146 \quad D_\gamma = e^{H_\gamma}, \quad (9)$$

147 With the above information, the dispersion of BC particle mixing states can be defined as

$$148 \quad \chi = \frac{D_\alpha - 1}{D_\gamma - 1}. \quad (10)$$



149 The basic idea of quantifying the BC particle mixing states is the same as that of Riemer and
150 West (2013) and Riemer et al. (2019), their framework mainly focuses on the bulk ambient aerosols
151 with about five species (Bondy et al., 2018; Ye et al., 2018). Our developed χ is a reduced parameter
152 that only concerns the BC-containing aerosols with two species of BC component and non-BC
153 coating materials.

154 3. Results and Discussions

155 3.1 BC mixing states diagram

156 A mixing state diagram as shown in Fig. 2 was employed for better understanding the dispersion
157 of BC mixing states. Nine different group bulks of aerosols were given and summarized in Table 1.
158 For each group, we include six BC-containing particles with different mass concentrations of BC
159 core and non-BC coating material.

160 For group 1, the amounts of BC are very small (near zero) and most of the aerosols are
161 composed of the non-BC component. The D_α and D_γ values are 1.00 and 1.00 respectively. These
162 groups can also be described as all of the particles are pure BC particles without coating.

163 For groups 2, 3, and 4, the mass concentration ratios of the BC component to the non-BC
164 component are 1:5, 2:4, and 3:3 respectively. All of the D_α values are 1.00 for groups 2, 3, and 4
165 because the BC particles are externally mixed. The corresponding D_γ values are 1.56, 1.89, and
166 2.00 respectively. For these three groups, the χ values are all 0.00.

167 For groups 4, 5, 6, and 7, the mass concentration ratios of the BC component to the non-BC
168 component are all 1:1 while the BC component is mixed to a different extent. It is easy to conclude
169 that the BC particles of group 7 are most well mixed among these four groups. The corresponding χ
170 values are 0, 0.26, 0.83, and 1.0 for group 4, 5, 6, and 7, respectively.

171 As for groups 8 and 9, the mass concentration ratios of the BC component to the non-BC
172 component are 1:6.1. The D_γ values are 1.5 and the D_α values are 1.5 and 1.35 respectively.

173 From the different group, the average particle species diversity D_γ value is mainly determined
174 by the total mass concentration ratio of the BC component to the non-BC component. It varies



175 between 1 and 2 for different total mass concentration ratios. The D_γ increases when the mass ratio
176 approaches 1. The bulk population species diversity D_α ranges between 1 and D_γ . It denotes the
177 diversity of different BC-containing particles.

178 3.2 Overview of the measurement

179 Fig.S6 gives the time series of our field measurements results. During the field measurement, the
180 σ_{sca} varies between 29 and 1590 Mm^{-1} . The ranges of H_α , H_γ , D_α , D_γ , and χ are 0.10~0.55,
181 0.42~0.64, 1.32~1.72, 1.52~1.91 and 0.62~0.82 respectively.

182 For a better understanding of the characteristics of the above parameters, we only present the
183 time series of these parameters during a pollution period between 27, May and 30, May in Fig. 3. As
184 shown in Fig. 3, the MR increased from about 2 to 4 when the σ_{sca} increased from 300 to 1200
185 Mm^{-1} , which indicates that some secondary aerosol components were coated on the BC particles
186 when the ambient air is more polluted. During the aging processing, the H_α decreased from 0.51 to
187 0.38 and H_γ decreased from 0.63 to 0.49. The D_α decreases with the MR from 1.66 to 1.48, which
188 is consistent with the results in section 3.1 that the D_α should decrease with the MR when the MR is
189 larger than 1. The χ varies between 0.68 and 0.79. It is worth noting that the χ is not well correlated
190 with the pollution conditions.

191 The daily variation of σ_{sca} , which is highly related to the development of the boundary layer,
192 reaches its maximum value of 525 Mm^{-1} at 6:00 AM and a minimum value of 150 Mm at 7:00 PM.
193 The daily variation of MR is largest at 5:00 AM with a mean value of 3.16 and reaches its minimum
194 value of 2.56 at 7:00 PM. The daily variation of MR was mainly influenced by aging processing and
195 anthropogenic activities. During the daytime, the newly emitted BC particles due to anthropogenic
196 activities have low MR and the measured mean MR is low than that at night. The D_α values, which
197 are anti-correlated with MR, show the opposite trend with MR. As for χ , it is smaller in the daytime
198 than that at night. The lower χ values at daytime mainly resulted from the mixing of newly emitted
199 BC particles due to anthropogenic activities and some pre-existed aged BC particles.



200 3.3 Relationship between the χ and E_{abs} from measurement

201 For each of the measured group of size-resolved BC mixing states, we calculated the
202 corresponding MR, χ , and E_{abs} . And the relationship between the MR and absorption enhancement
203 is summarized in Fig. 5. Overall, the BC E_{abs} increase with MR, which is consistent with the
204 previous knowledge. For a given value of MR, E_{abs} varies by about 20%, especially for these
205 conditions with MR larger than 1.0. When MR is larger than 1.0, the E_{abs} increase with the χ .
206 Relationship between the E_{abs} and χ is rather complex when MR is smaller than 1.0. However, only
207 448 of 6948 groups (6.4%) of the measured MR values are smaller than 1. Therefore, for most of the
208 conditions, the measured E_{abs} should increase with χ , which indicates that the refractive index of χ
209 can be employed as a factor to constrain the E_{abs} of ambient aerosols.

210 A schematic diagram as shown in Fig. 6 to denotes the relationship between the E_{abs} and χ .
211 From Fig. 6, we calculated the E_{abs} and χ under differ MR and then compared the E_{abs} of different
212 bulk aerosols. The first group contains two particles with both the MR equaling 8. The corresponding
213 χ is 1.00 and E_{abs} is 1.60. Another group of particles contains two particles with MR equaling 1 and
214 15, respectively. Thus the second group of particles has a mean MR of 8. The calculated
215 corresponding χ and E_{abs} are 0.79 and 1.42 respectively. Thus, the E_{abs} tend to increase with χ for
216 the same MR, which is mainly resulted from that the increasing ratio of E_{abs} (the slope of E_{abs} to
217 MR) decrease with MR.

218 It is worth noting that the increasing ratio is almost the same when the MR is in the range of 0
219 and 3. Therefore, the E_{abs} doesn't tend to increase with the χ when the MR was less than 1, which
220 is consistent with our study as shown in Fig. 6.

221 3.4 Relationship between the χ and E_{abs} from simulation

222 A Mont-Carlo simulation was carried out for a better understanding of the relationship between
223 χ and E_{abs} . During the simulation, the number of BC-containing particles was assumed to be 30. For
224 each of the BC particle, the core diameter of the BC particle was randomly generated with a
225 geometric mean diameter of 130.7 nm and a geometric standard deviation of 1.5, which is the mean



226 measurement results of the BC core distribution during the field measurement (Zhao et al., 2020b).
227 The corresponding MR of the BC particle is assumed to be in the range between 0.0 (pure BC
228 particles without coating) and 78.0 (particles with a core diameter of 130 nm and a total diameter of
229 560 nm). For each of the group of particles, the corresponding aerosol bulk MR, E_{abs} and χ can be
230 calculated. The simulations were conducted for 10^7 times, and the calculated mean and standard
231 deviation of E_{abs} under different MR and χ are summarized in Fig. 7 (a) and (b).

232 From Fig. 7 (a), the calculated E_{abs} tend to increase with MR for each of the given χ , which is
233 consistent with the previous knowledge of the BC light absorption properties. Then the MR is
234 smaller than 2, the calculated E_{abs} does not seem to increase with the χ , which is consistent with the
235 analyzed results from section 3.3 and Fig. 6. When the MR is larger 2, the E_{abs} tend to increase
236 with the χ . The larger the MR is, the E_{abs} is more sensitive to χ . Two reasons may lead to this
237 phenomenon. One reason is that that calculated slope of E_{abs} to MR for one particle as shown in Fig.
238 6 decreases with the MR. Another reason is that the calculated E_{abs} range increase with MR when
239 the χ changes between 0 and 1 as shown in Fig. 5.

240 As for the uncertainties of simulated E_{abs} , it tends to increase with the MR, which is consistent
241 with the previous discussions that the E_{abs} the range tends to increase with MR. Overall, the
242 calculated standard deviations of E_{abs} are all the way smaller than 10% for different MR and χ .
243 Therefore, the calculated E_{abs} can be well constrained by χ .

244 4 Conclusion

245 Larger uncertainties remain when estimating the warming effects of ambient BC aerosols due to
246 the poor understanding of the ambient BC light absorption enhance ratio. Previous studies find that
247 the light absorption of ambient aerosols was mainly determined by the morphology of the BC core,
248 the position of the BC core inside coating, the coating thickness, and the size distribution of the BC.
249 We find that there are more than 20% of uncertainties for the same measured mean coating thickness,
250 i.e. the same measured MR based on the field measurement of the size-resolved BC mixing states.
251 However, there were no-study, to our best knowledge, that attempts to constrain the uncertainties.



252 In this study, we developed the BC mixing states index χ based on the mass concentrations of
253 BC components and non-BC material of each BC-containing particle. Results show that the light
254 absorption enhancement ratio E_{abs} tend to increase the χ for the same measured MR. Therefore, our
255 developed parameter χ , which reflects the dispersion of the BC mixing states, can be employed as an
256 effective parameter to constrain the light absorption enhancement of ambient BC-containing
257 aerosols.

258

259 **Data availability.** The data involved is available in the manuscript.

260 **Author contributions.** Gang Zhao wrote the manuscript. Chunsheng Zhao, Min Hu, Tianyi Tan,
261 Song Guo, Zhijun Wu, Yishu Zhu and Gang Zhao discussed the results.

262 **Competing interests.** The authors declare that they have no conflict of interest.

263 **Acknowledgments.** This work is supported by the National Key R&D Program of China
264 (2016YFC020000: Task 5) and the National Natural Science Foundation of China (41590872).

265

266

267

268



-
- 269 Bohren, C. F., and Huffman, D. R.: Absorption and Scattering by a Sphere, in Absorption and
270 Scattering of Light by Small Particles, Wiley-VCH Verlag GmbH, 82-129, 2007.
- 271 Bond, T. C., and Bergstrom, R. W.: Light Absorption by Carbonaceous Particles: An Investigative
272 Review, *Aerosol Sci. Technol.*, 40, 27-67, 10.1080/02786820500421521, 2006.
- 273 Bond, T. C., Doherty, S. J., Fahey, D. W., Forster, P. M., Berntsen, T., DeAngelo, B. J., Flanner, M.
274 G., Ghan, S., Karcher, B., Koch, D., Kinne, S., Kondo, Y., Quinn, P. K., Sarofim, M. C., Schultz, M.
275 G., Schulz, M., Venkataraman, C., Zhang, H., Zhang, S., Bellouin, N., Guttikunda, S. K., Hopke, P.
276 K., Jacobson, M. Z., Kaiser, J. W., Klimont, Z., Lohmann, U., Schwarz, J. P., Shindell, D.,
277 Storelvmo, T., Warren, S. G., and Zender, C. S.: Bounding the role of black carbon in the climate
278 system: A scientific assessment, *J Geophys Res-Atmos*, 118, 5380-5552, 10.1002/jgrd.50171, 2013.
- 279 Bondy, A. L., Bonanno, D., Moffet, R. C., Wang, B., Laskin, A., and Ault, A. P.: The diverse
280 chemical mixing state of aerosol particles in the southeastern United States, *Atmospheric Chemistry
281 and Physics*, 18, 12595-12612, 10.5194/acp-18-12595-2018, 2018.
- 282 Cappa, C. D., Onasch, T. B., Massoli, P., Worsnop, D. R., Bates, T. S., Cross, E. S., Davidovits, P.,
283 Hakala, J., Hayden, K. L., Jobson, B. T., Kolesar, K. R., Lack, D. A., Lerner, B. M., Li, S. M.,
284 Mellon, D., Nuaaman, I., Olfert, J. S., Petaja, T., Quinn, P. K., Song, C., Subramanian, R., Williams,
285 E. J., and Zaveri, R. A.: Radiative Absorption Enhancements Due to the Mixing State of
286 Atmospheric Black Carbon, *Science*, 337, 1078-1081, 10.1126/science.1223447, 2012.
- 287 Cappa, C. D., Zhang, X., Russell, L. M., Collier, S., Lee, A. K. Y., Chen, C.-L., Betha, R., Chen, S.,
288 Liu, J., Price, D. J., Sanchez, K. J., McMeeking, G. R., Williams, L. R., Onasch, T. B., Worsnop, D.
289 R., Abbatt, J., and Zhang, Q.: Light Absorption by Ambient Black and Brown Carbon and its
290 Dependence on Black Carbon Coating State for Two California, USA, Cities in Winter and Summer,
291 *Journal of Geophysical Research: Atmospheres*, 124, 1550-1577, 10.1029/2018jd029501, 2019.
- 292 Cui, X., Wang, X., Yang, L., Chen, B., Chen, J., Andersson, A., and Gustafsson, Ö.: Radiative
293 absorption enhancement from coatings on black carbon aerosols, *Science of The Total Environment*,
294 551-552, 51-56, doi.org/10.1016/j.scitotenv.2016.02.026, 2016.



-
- 295 Fierce, L., Bond, T. C., Bauer, S. E., Mena, F., and Riemer, N.: Black carbon absorption at the global
296 scale is affected by particle-scale diversity in composition, *Nature communications*, 7, 12361,
297 10.1038/ncomms12361, 2016.
- 298 Fierce, L., Onasch, T. B., Cappa, C. D., Mazzoleni, C., China, S., Bhandari, J., Davidovits, P.,
299 Fischer, D. A., Helgestad, T., Lambe, A. T., Sedlacek, A. J., 3rd, Smith, G. D., and Wolff, L.:
300 Radiative absorption enhancements by black carbon controlled by particle-to-particle heterogeneity
301 in composition, *Proceedings of the National Academy of Sciences of the United States of America*,
302 117, 5196-5203, 10.1073/pnas.1919723117, 2020.
- 303 Jacobson, M. Z.: Short-term effects of controlling fossil-fuel soot, biofuel soot and gases, and
304 methane on climate, Arctic ice, and air pollution health, *Journal of Geophysical Research:*
305 *Atmospheres*, 115, n/a-n/a, 10.1029/2009JD013795, 2010.
- 306 Koch, D., Schulz, M., Kinne, S., and McNaughton, C.: Evaluation of black carbon estimations in
307 global aerosol models, *Atmospheric Chemistry & Physics*, 9, 9001-9026, 2009.
- 308 Lan, Z.-J., Huang, X.-F., Yu, K.-Y., Sun, T.-L., Zeng, L.-W., and Hu, M.: Light absorption of black
309 carbon aerosol and its enhancement by mixing state in an urban atmosphere in South China,
310 *Atmospheric Environment*, 69, 118-123, 10.1016/j.atmosenv.2012.12.009, 2013.
- 311 Liu, D., Allan, J. D., Young, D. E., Coe, H., Beddows, D., Fleming, Z. L., Flynn, M. J., Gallagher, M.
312 W., Harrison, R. M., Lee, J., Prevot, A. S. H., Taylor, J. W., Yin, J., Williams, P. I., and Zotter, P.:
313 Size distribution, mixing state and source apportionment of black carbon aerosol in London during
314 wintertime, *Atmospheric Chemistry and Physics*, 14, 10061-10084, 10.5194/acp-14-10061-2014,
315 2014.
- 316 Liu, D., Whitehead, J., Alfarra, M. R., Reyes-Villegas, E., Spracklen, Dominick V., Reddington,
317 Carly L., Kong, S., Williams, Paul I., Ting, Y.-C., Haslett, S., Taylor, Jonathan W., Flynn, Michael J.,
318 Morgan, William T., McFiggans, G., Coe, H., and Allan, James D.: Black-carbon absorption
319 enhancement in the atmosphere determined by particle mixing state, *Nature Geoscience*, 10, 184-188,
320 10.1038/ngeo2901, 2017.



-
- 321 Liu, J., Li, X., Li, D., Xu, R., Gao, Y., Chen, S., Liu, Y., Zhao, G., Wang, H., Wang, H., Lou, S.,
322 Chen, M., Hu, J., Lu, K., Wu, Z., Hu, M., Zeng, L., and Zhang, Y.: Observations of glyoxal and
323 methylglyoxal in a suburban area of the Yangtze River Delta, China, *Atmospheric Environment*, 238,
324 117727, 10.1016/j.atmosenv.2020.117727, 2020.
- 325 Liu, S., Aiken, A. C., Gorkowski, K., Dubey, M. K., Cappa, C. D., Williams, L. R., Herndon, S. C.,
326 Massoli, P., Fortner, E. C., Chhabra, P. S., Brooks, W. A., Onasch, T. B., Jayne, J. T., Worsnop, D.
327 R., China, S., Sharma, N., Mazzoleni, C., Xu, L., Ng, N. L., Liu, D., Allan, J. D., Lee, J. D., Fleming,
328 Z. L., Mohr, C., Zotter, P., Szidat, S., and Prevot, A. S.: Enhanced light absorption by mixed source
329 black and brown carbon particles in UK winter, *Nature communications*, 6, 8435,
330 10.1038/ncomms9435, 2015.
- 331 Menon, S., Hansen, J., Nazarenko, L., and Luo, Y.: Climate effects of black carbon aerosols in China
332 and India, *Science*, 297, 2250-2253, 10.1126/science.1075159, 2002.
- 333 Müller, T., Laborde, M., Kassell, G., and Wiedensohler, A.: Design and performance of a
334 three-wavelength LED-based total scatter and backscatter integrating nephelometer, *Atmos. Meas.*
335 *Tech.*, 4, 1291-1303, 10.5194/amt-4-1291-2011, 2011.
- 336 Nakayama, T., Ikeda, Y., Sawada, Y., Setoguchi, Y., Ogawa, S., Kawana, K., Mochida, M., Ikemori,
337 F., Matsumoto, K., and Matsumi, Y.: Properties of light-absorbing aerosols in the Nagoya urban area,
338 Japan, in August 2011 and January 2012: Contributions of brown carbon and lensing effect, *Journal*
339 *of Geophysical Research: Atmospheres*, 119, 12,721-712,739, 10.1002/2014JD021744, 2014.
- 340 Peng, J., Hu, M., Guo, S., Du, Z., Zheng, J., Shang, D., Levy Zamora, M., Zeng, L., Shao, M., Wu,
341 Y.-S., Zheng, J., Wang, Y., Glen, C. R., Collins, D. R., Molina, M. J., and Zhang, R.: Markedly
342 enhanced absorption and direct radiative forcing of black carbon under polluted urban environments,
343 *Proceedings of the National Academy of Sciences*, 113, 4266-4271, 10.1073/pnas.1602310113,
344 2016.
- 345 Peng, J., Hu, M., Guo, S., Du, Z., Shang, D., Zheng, J., Zheng, J., Zeng, L., Shao, M., Wu, Y.,
346 Collins, D., and Zhang, R.: Ageing and hygroscopicity variation of black carbon particles in Beijing



347 measured by a quasi-atmospheric aerosol evolution study (QUALITY) chamber, Atmospheric
348 Chemistry and Physics, 17, 10333-10348, 10.5194/acp-17-10333-2017, 2017.

349 Riemer, N., and West, M.: Quantifying aerosol mixing state with entropy and diversity measures,
350 Atmospheric Chemistry and Physics, 13, 11423-11439, 10.5194/acp-13-11423-2013, 2013.

351 Riemer, N., Ault, A. P., West, M., Craig, R. L., and Curtis, J. H.: Aerosol Mixing State:
352 Measurements, Modeling, and Impacts, Reviews of Geophysics, 57, 187-249,
353 10.1029/2018rg000615, 2019.

354 Saleh, R., Hennigan, C. J., McMeeking, G. R., Chuang, W. K., Robinson, E. S., Coe, H., Donahue, N.
355 M., and Robinson, A. L.: Absorptivity of brown carbon in fresh and photo-chemically aged
356 biomass-burning emissions, Atmos. Chem. Phys., 13, 7683-7693, 10.5194/acp-13-7683-2013, 2013.

357 Saleh, R., Robinson, E. S., Tkacik, D. S., Ahern, A. T., Liu, S., Aiken, A. C., Sullivan, R. C., Presto,
358 A. A., Dubey, M. K., Yokelson, R. J., Donahue, N. M., and Robinson, A. L.: Brownness of organics
359 in aerosols from biomass burning linked to their black carbon content, Nature Geoscience, 7, 647,
360 10.1038/ngeo2220, 2014.

361 Wu, Y., Cheng, T., Liu, D., Allan, J. D., Zheng, L., and Chen, H.: Light Absorption Enhancement of
362 Black Carbon Aerosol Constrained by Particle Morphology, Environ Sci Technol, 52, 6912-6919,
363 10.1021/acs.est.8b00636, 2018.

364 Xie, C., Xu, W., Wang, J., Liu, D., Ge, X., Zhang, Q., Wang, Q., Du, W., Zhao, J., Zhou, W., Li, J.,
365 Fu, P., Wang, Z., Worsnop, D., and Sun, Y.: Light absorption enhancement of black carbon in urban
366 Beijing in summer, Atmospheric Environment, 10.1016/j.atmosenv.2019.06.041, 2019.

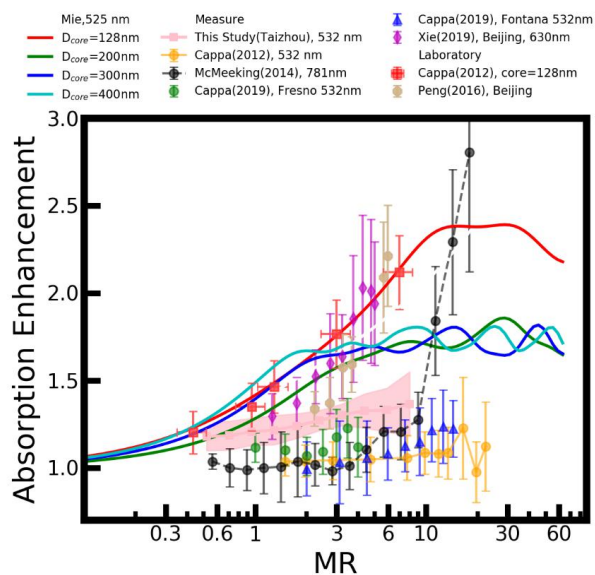
367 Ye, Q., Gu, P., Li, H. Z., Robinson, E. S., Lipsky, E., Kaltsonoudis, C., Lee, A. K. Y., Apte, J. S.,
368 Robinson, A. L., Sullivan, R. C., Presto, A. A., and Donahue, N. M.: Spatial Variability of Sources
369 and Mixing State of Atmospheric Particles in a Metropolitan Area, Environ Sci Technol, 52,
370 6807-6815, 10.1021/acs.est.8b01011, 2018.



-
- 371 Yuan, C., Zheng, J., Ma, Y., Jiang, Y., Li, Y., and Wang, Z.: Significant restructuring and light
372 absorption enhancement of black carbon particles by ammonium nitrate coating, *Environ Pollut*, 262,
373 114172, 10.1016/j.envpol.2020.114172, 2020.
- 374 Zhang, X., Mao, M., Yin, Y., and Wang, B.: Absorption enhancement of aged black carbon aerosols
375 affected by their microphysics: a numerical investigation, *Journal of Quantitative Spectroscopy and*
376 *Radiative Transfer*, 202, 90-97, 10.1016/j.jqsrt.2017.07.025, 2017.
- 377 Zhao, G., Tan, T., Zhao, W., Guo, S., Tian, P., and Zhao, C.: A new parameterization scheme for the
378 real part of the ambient urban aerosol refractive index, *Atmos. Chem. Phys.*, 19, 12875-12885,
379 10.5194/acp-19-12875-2019, 2019a.
- 380 Zhao, G., Tao, J., Kuang, Y., Shen, C., Yu, Y., and Zhao, C.: Role of black carbon mass size
381 distribution in the direct aerosol radiative forcing, *Atmos. Chem. Phys.*, 19, 13175-13188,
382 10.5194/acp-19-13175-2019, 2019b.
- 383 Zhao, G., Zhao, W., and Zhao, C.: Method to measure the size-resolved real part of aerosol refractive
384 index using differential mobility analyzer in tandem with single-particle soot photometer,
385 *Atmospheric Measurement Techniques*, 12, 3541-3550, 10.5194/amt-12-3541-2019, 2019c.
- 386 Zhao, G., Li, F., and Zhao, C.: Determination of the refractive index of ambient aerosols,
387 *Atmospheric Environment*, 240, 117800, 10.1016/j.atmosenv.2020.117800, 2020a.
- 388 Zhao, G., Shen, C., and Zhao, C.: Technical note: Mismeasurement of the core-shell structure of
389 black carbon-containing ambient aerosols by SP2 measurements, *Atmospheric Environment*, 243,
390 117885, 10.1016/j.atmosenv.2020.117885, 2020b.

391

392

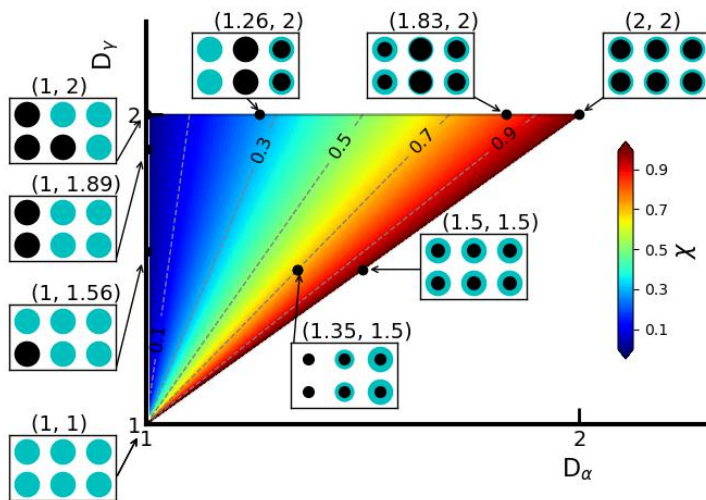


393

394 Figure 1. The measured E_{abs} of BC particles from different ambient measurements, including this

395 work (in pink), and lab studies.

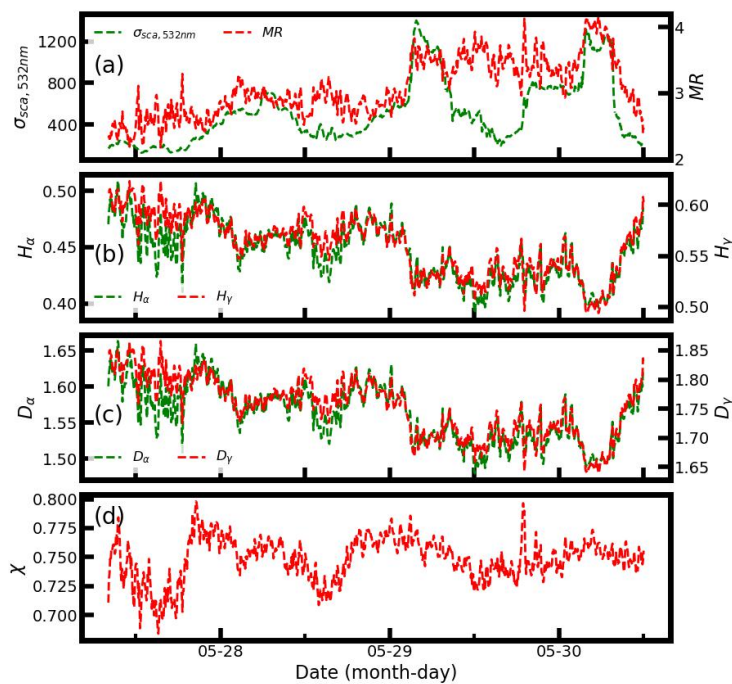
396



397

398 **Figure 2.** Mixing states diagram to illustrate the relationship between D_α , D_γ , and χ . Each species
399 consists of six particles, and the colors of black and cyan represent the BC and non-BC components.

400

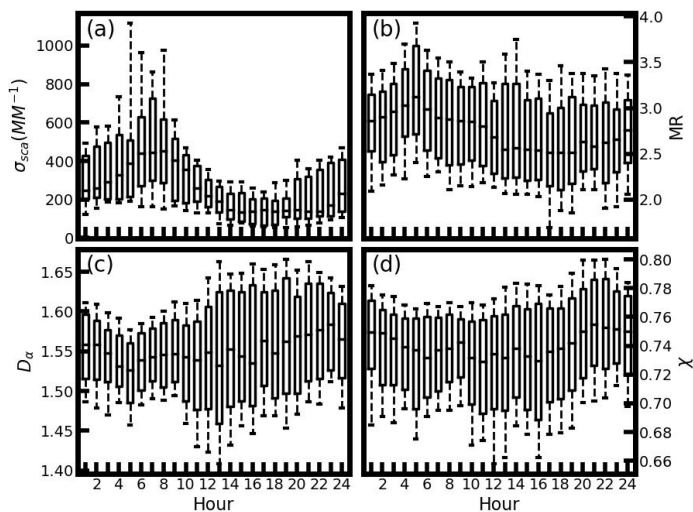


401

402

Figure 3. Measured time series of (a) σ_{sca} and MR, (b) H_α and H_γ , (c) D_α and D_γ , and (d) χ .

403



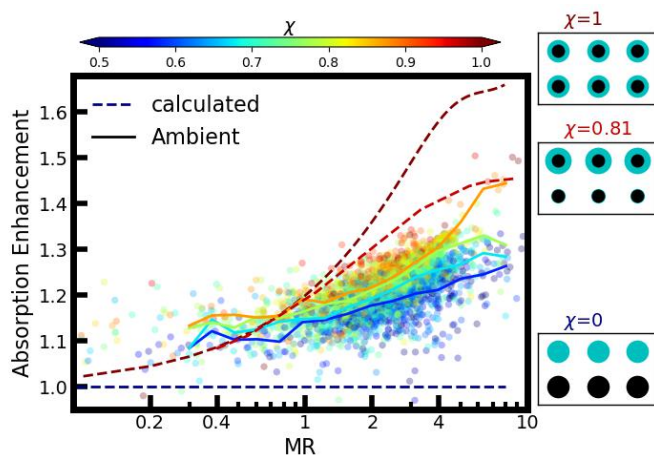
404

405

Figure 4. Daily variation of the measured (a) σ_{sca} , (b) MR, (c) D_α , and (d) χ .

406

407

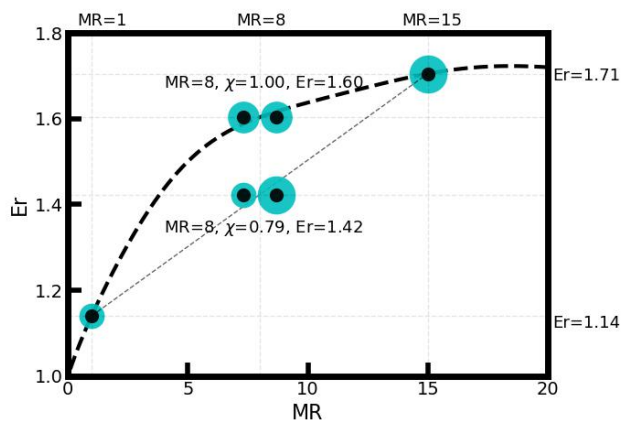


408

409

Figure 5. Relationship between the BC E_{abs} and the measured mass ratio of the BC-containing aerosols coating material to BC under different χ conditions. Four solid lines from bottom to up corresponding to the measured ambient size-resolved BC mixing states data with χ ranges of 0.575~0.625, 0.625~0.675, 0.675~0.725, and 0.725~0.775. The dotted line corresponds to the χ of 0.0 (blue), 0.81 (light red), and 1.0 (dark red), respectively.

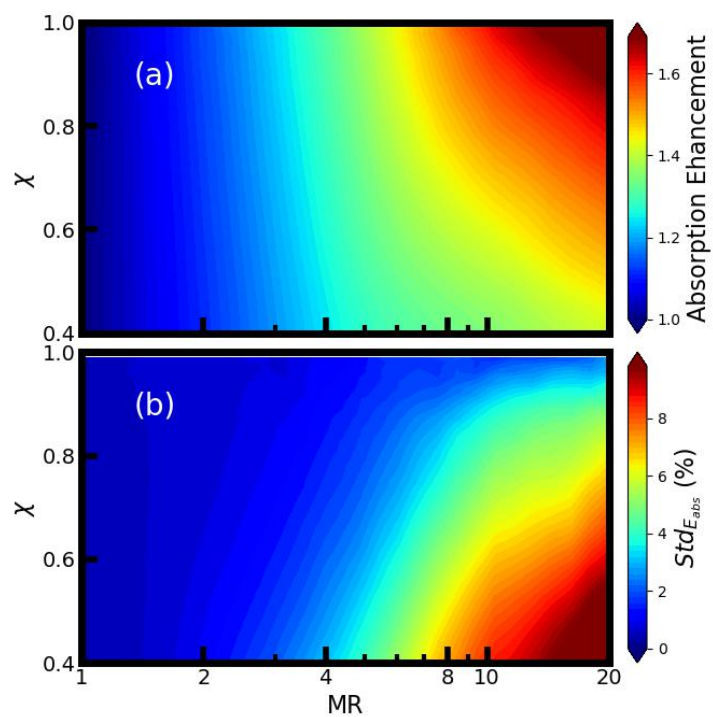
414



415

416 **Figure 6.** Schematic diagram that denotes the relationship between χ and Er.

417



418

419 **Figure 7.** The calculated (a) mean E_{abs} values and (b) standard deviations of the E_{abs} values for
420 different MR and χ .



ID	(D_α, D_γ)	χ	P1* ¹	P2* ¹	P3* ¹	P4* ¹	P5* ¹	P6* ¹	Tot* ¹
1	(1.00, 1.00)	-	(0, 1)	(0, 1)	(0, 1)	(0, 1)	(0, 1)	(0, 1)	(0, 6)
2	(1.00, 1.56)	0	(1, 0)	(0, 1)	(0, 1)	(0, 1)	(0, 1)	(0, 1)	(1, 5)
3	(1.00, 1.89)	0	(1, 0)	(1, 0)	(0, 1)	(0, 1)	(0, 1)	(0, 1)	(2, 4)
4	(1.00, 2.00)	0	(1, 0)	(1, 0)	(1, 0)	(0, 1)	(0, 1)	(0, 1)	(3, 3)
5	(1.26, 2.00)	0.26	(2, 0)	(2, 0)	(0, 2)	(0, 2)	(1, 1)	(1, 1)	(6, 6)
6	(1.83, 2.00)	0.83	(1, 3)	(1, 3)	(3, 1)	(3, 1)	(2, 2)	(2, 2)	(12, 12)
7	(2.00, 2.00)	1.00	(1, 1)	(1, 1)	(1, 1)	(1, 1)	(1, 1)	(1, 1)	(6, 6)
8	(1.5, 1.50)	1.00	(1, 6.1)	(1, 6.1)	(1, 6.1)	(1, 6.1)	(1, 6.1)	(1, 6.1)	(6, 36.6)
9	(1.35, 1.50)	0.70	(1, 0)	(1, 0)	(1, 6.1)	(1, 6.1)	(1, 12.2)	(1, 12.2)	(6, 36.6)

Table 1.
 Detail information of the BC particle

s shown in Fig.2

430

431

432

433

434

435

436

*¹ Mass of the BC component of and non-BC component (arbitrary unit).